The linearized CREATE-L plasma response model for the control of current, position and shape in tokamaks



1998 Nucl. Fusion 38 723

(http://iopscience.iop.org/0029-5515/38/5/307)

# THE LINEARIZED CREATE-L PLASMA RESPONSE MODEL FOR THE CONTROL OF CURRENT, POSITION AND SHAPE IN TOKAMAKS

R. ALBANESE
Associazione Euratom–ENEA–CREATE,
DIMET, Università degli Studi di Reggio Calabria,
Reggio Calabria

F. VILLONE
Associazione Euratom–ENEA–CREATE,
DII, Università degli Studi di Cassino,
Cassino

Italy

ABSTRACT. CREATE-L, a simple and reliable linearized plasma response model for the control of the plasma current, position and shape in tokamaks, is presented. The basic assumption made is that the plasma behaviour is described using three degrees of freedom, related to the total plasma current, internal inductance and poloidal beta. The state variables are the coil and plasma currents; the inputs are the applied voltages, whereas poloidal beta and internal inductance play the role of disturbances. The outputs are field and flux values and some basic plasma parameters. The model is tested against non-linear codes and validated via comparison with experimental results.

## 1. INTRODUCTION

The control of plasma current, position and shape in a tokamak is usually carried out on the basis of simple models [1–3]. For some parameters it is even possible to assume that the plasma response to external inputs is independent of the plasma itself, as the system is largely dominated by electromagnetic effects [3]. On the basis of these assumptions, it is possible to design a control system able to meet the control requirements in present physics experiments.

Better performance must be achieved by the control systems in future tokamaks, in which ignition requires the avoidance of any contact between the plasma and the wall. For future devices such as ITER [4], it will probably be necessary to use modern and sophisticated control techniques such as LQG-LTR [5] or $H_\infty$ [6], with rather stringent safety margins in terms of coil voltages and currents, electric power, thermal and electromagnetic loads, for example.

There exist several non-linear plasma simulation codes that have been tested against present experiments, for example those presented in Refs [7, 8]. They provide simulation environments that can be used to check the performance of a control system. However, they are difficult to apply for routine use in controller design and performance analysis. This is mainly due to the long computer time needed for the simulation and the difficulty of deriving the linearized form usually needed for controller design. For this reason, the need for a simple but reliable plasma response model has become strong.

Several linearized models have been proposed in the literature. Most of them are based on simplifying assumptions that dramatically reduce the dimensionality of the system.

In models and associated codes in which the basic unknown is the plasma displacement, such as ERATO [9], the main objective is to assess the MHD stability of a plasma configuration. For this reason, the surrounding structures are assumed to be ideally conducting, so that these tools cannot be used for plasma control. This limitation has been removed in the NOVA-W stability code [10], which works in the frequency domain. Like most MHD stability codes, NOVA-W is well suited for limiter configurations; its application to diverted plasmas is obtained via extrapolation.

The models initially used for plasma control included more or less detailed circuit equations for both active and passive conductors, but treated the plasma in an approximate fashion, often as a set of filamentary coils with a prescribed, usually rigid, motion [1, 2].

A typical assumption widely used in linear models is to neglect the plasma mass on the time-scale on which the control system works. In this way, the plasma is assumed to evolve through a sequence of MHD equilibria. This is the main basis for the perturbed equilibrium models, first introduced in Ref. [11] and later extended to include the effects of approximate flux conservation [12, 13]. The CREATE-L model described in the present article falls into this class of model, and is the natural evolution of the technique presented in Ref. [11].

The perturbed equilibrium models have also been used with additional simplifying assumptions. The contribution of the eddy currents in the passive structures has often been disregarded [14]. There is also the plasmaless model proposed in Ref. [3], which has the undeniable advantage of being independent of plasma configuration, but is of course unable to predict some open loop characteristics of the plasma, such as the growth rate of the vertical instability.

The article is organized as follows. Section 2 illustrates the assumptions and equations for the linearized CREATE-L plasma response model. Section 3 discusses the validation of the model in comparison with non-linear codes and experimental results. Finally, Section 4 reports the main conclusions.

## 2. THE OPEN LOOP PLASMA RESPONSE MODEL

### 2.1. Assumptions

The main application of the linearized open loop plasma response model is for the design of the plasma current, position and shape control system. For this reason, the time-scale of interest is much longer than the Alfvén time and therefore the plasma can be assumed to evolve through a sequence of MHD equilibria, i.e. to be massless.

Another basic assumption we make is that the plasma behaviour can be described using a small number of degrees of freedom. From the knowledge of external magnetic measurements, it is possible to identify a number of plasma parameters, including the total plasma current, the position of the plasma current centroid and, in some cases, the shape of the plasma separatrix, the poloidal beta and the internal inductance. However, additional information on the current density profile is difficult to obtain from external magnetic measurements. Therefore, we assume that the three parameters $I_\mathrm{p}$ (total plasma current), $l_\mathrm{i}$ (internal inductance) and $\beta_\mathrm{p}$ (poloidal beta) provide a sufficient basis for representing plasma equilibria [15]. Of course, this does not mean that other plasma parameters are unimportant for purposes different from current, position and shape control.

The Grad–Shafranov equation provides the following expression for the plasma current density:

$$J_{\mathrm{p}\varphi} = r\,\mathrm{d}p/\mathrm{d}\psi + (f\,\mathrm{d}f/\mathrm{d}\psi)/\mu_0 r \qquad (1)$$

where $J_{\mathrm{p}\varphi}$ is the toroidal component of the plasma current density, $r$ the radial co-ordinate, $p$ the pressure, $\psi$ the poloidal magnetic flux per radian, $f/r$ the toroidal component of the flux density and $\mu_0$ the vacuum magnetic permeability.

Following Ref. [15], we assume the plasma current density profile to be a function of four parameters ($\lambda$, $\beta_0$, $\alpha_m$ and $\alpha_n$) that can be associated with the physical quantities $I_\mathrm{p}$, $\beta_\mathrm{p}$, $l_\mathrm{i}$ and $q_0$ (safety factor at magnetic axis):

$$J_{\mathrm{p}\varphi} = \lambda[\beta_0 r/R_0 + (1-\beta_0)R_0/r]j(\bar{\psi}, \alpha_m, \alpha_n) \qquad (2)$$

with $\bar{\psi} = (\psi - \psi_\mathrm{a})/(\psi_\mathrm{b} - \psi_\mathrm{a})$, where $\psi_\mathrm{a}$ is the flux per radian at the plasma magnetic axis, $\psi_\mathrm{b}$ the flux per radian at the plasma boundary, $j$ a suitable function and $R_0$ a reference length, for example the major radius of the vacuum chamber.

The results presented in this article have been obtained by selecting $j = (1 - \bar{\psi}^{\alpha_m})^{\alpha_n}$. With this choice, the current density at the plasma boundary is automatically zero, $I_\mathrm{p}$ is mainly related to $\lambda$, $\beta_\mathrm{p}$ is basically linked to $\beta_0$, and the internal inductance and the safety factor depend on the values of $\alpha_m$ and $\alpha_n$. However, in our dynamical model we will vary only three linear combinations of the plasma profile parameters $\lambda$, $\beta_0$, $\alpha_m$ and $\alpha_n$, since the influence of $q_0$ on the electromagnetic interaction between plasma and external currents is negligible.

The fundamental idea is to treat the variations of $l_\mathrm{i}$ and $\beta_\mathrm{p}$ as disturbances. For this reason, in the absence of any disturbances, the values of $\alpha_m$, $\alpha_n$ and $\beta_0$ are assumed to be constant throughout the whole evolution. In this way, $l_\mathrm{i}$ and $\beta_\mathrm{p}$ remain roughly constant. On the other hand, although the plasma current density profile is held fixed, the total plasma current $I_\mathrm{p}$ is not kept constant, as the time evolution of the $\lambda$ parameter is determined taking into account Ohm's law in the plasma region. In this way, the plasma current density profile variations are not taken into account self-consistently. This is not critical when dealing with slow changes driven by the external currents. However, we cannot take the fast internal disturbances properly into account.

In this way, the time evolution of the magnetic field is determined by solving the free boundary equilibrium problem coupled to the circuit equations for the external conductors and a similar equation for the total plasma current. Notice that, after discretization, a circuit approach can also be applied in the presence of conductive structures such as vacuum vessel and blanket [8, 16].

In our approach a prominent role is played by the energy stored in the magnetic field. The macroscopic kinetic energy, the radiative dissipation and the effects of nuclear reactions are completely neglected. The work done by pressure and the exchanges between toroidal and poloidal magnetic energy are taken into account instead.

Solving a free boundary problem we implicitly assume a sharp plasma–vacuum interface. The primary aim of the control problem is to keep the position and the shape of this interface close to a desired configuration. The boundary is assumed to be a flux surface, which is not completely defined without specifying the time evolution of its flux value. In ideal MHD the boundary flux is frozen throughout the whole evolution. Conversely, in evolutionary equilibrium models, the plasma boundary is usually defined as the outermost flux surface that does not intersect the wall, either tangential to the wall (limiter configurations) or with an X point (diverted configurations). With this assumption, in a diverted configuration, the plasma may happen to move towards the wall, switching to a limiter configuration. Equally well, in a limiter configuration, the plasma might also in principle detach from the wall. Of course, in experimental reality these problems are overcome, as no sharp plasma–vacuum interface exists and a region formed of low temperature plasma is present around the hot core [17].

Each of the two differing assumptions about the plasma boundary represents a limiting description of the real behaviour.

With the ideal MHD model if a limiter plasma moves away from the wall, the current density remains zero in the part of the region inside the outermost flux line that does not intersect the wall. If the plasma moves rapidly towards the wall, a poloidal current will flow through the first wall in the region between the hot core of the plasma and the magnetic surface corresponding to the initial plasma boundary flux. These 'attached' currents have been observed in the presence of vertical disruption events [18]. Therefore, the ideal MHD assumption about the plasma boundary is consistent with the hypothesis that the time-scale of our interest is short when compared with both the diffusion time and the decay time of the poloidal currents in the first wall. The diffusion time mainly depends on the plasma properties. The current in the first wall decays on a time-scale that mainly depends on the resistance of the poloidal path through the solid wall.

Therefore, for very fast phenomena, we might assume the flux at the plasma boundary to be frozen throughout the whole evolution. In the absence of other interactions, this choice would also imply energy conservation. Conversely, the assumption that the plasma boundary is given by the outermost closed surface in the chamber is valid for slow phenomena and implicitly involves exchanges or dissipation of energy. We take the latter as our reference assumption, because the main application of the plasma response model is the control of the plasma current, position and shape, typically characterized by a rather long time-scale.

Since CREATE-L is a model linearized around a reference configuration, we suppose that the time behaviour of the reference quantities is known a priori. Notice that the linearized model depends not only on the values of the reference quantities, but also on their derivatives. However, we are mainly interested in the flat-top phase, which is characterized by a rather slow dynamics. Therefore, in this article, we neglect the effects of nominal transients, i.e. we assume a time invariant model.

Finally, although the model allows the plasma resistivity to be properly taken into account by means of a global resistance, the results presented in this article are mostly based on the assumption that the ohmic dissipation inside the plasma is negligible. This choice is certainly valid in so far as the time-scale of the phenomena of interest is short in comparison with the electromagnetic time constant of the plasma. Near the plasma edge the current decay time-scale is rather shorter than it is in the hot core. Nevertheless, since at the edge the current is quite low, the overall electromagnetic effect is negligible. Of course, no fast internal disturbances are supposed to occur that strongly modify the current density profile as well as $l_i$ and $\beta_p$. As illustrated in Section 3, when a longer time-scale must be dealt with, experimental evidence shows that the main effect of the non-zero resistivity is a linear drift for some quantities. Hence, if this nominal linear transient is added to the modelled traces, the results provided by the model are accurate also in this case.

### 2.2. Model equations

Assuming axisymmetry, in a cylindrical coordinate system $(r, \varphi, z)$, the toroidal projection of Ampère's equation can be written as

$$L\psi = J_\varphi \tag{3}$$

where

$$L\psi = -\frac{\partial}{\partial r}\left(\frac{1}{\mu r}\frac{\partial \psi}{\partial r}\right) - \frac{\partial}{\partial z}\left(\frac{1}{\mu r}\frac{\partial \psi}{\partial z}\right)$$

$\mu$ is the magnetic permeability, $\psi$ the poloidal flux per radian and, finally, $J_\varphi$ the toroidal current density.

The solution domain includes the following zones: (a) plasma; (b) vacuum; (c) active coils, i.e. poloidal field (PF) and ohmic heating (OH) coils; (d) passive coils and conducting structures. The only difference between the two groups of conductors is the way they are fed: the applied voltage is zero for passive coils. The passive structures can also be schematized as a number of passive (short circuited) conductors [16, 18].

The expression for the toroidal current density in Eq. (3) takes different forms in the various zones of the solution domain. In the conductors, using the loop current method, we assume that

$$J_\varphi = \sum_{k=1}^{n} I_k J_{k\varphi}(r, z) \tag{4}$$

where $n$ is the number of independent loop currents and $J_{k\varphi}$ the toroidal component of the current density distribution $\boldsymbol{J}_k$ associated with the $k$th loop current $I_k$.

Inside the plasma region, we assume the expression for $J_\varphi$ to be given by Eq. (2), which involves the determination of the $\lambda$ parameter, which accounts for the total toroidal plasma current $I_\mathrm{p}$, as well as $\psi_\mathrm{a}$ and $\psi_\mathrm{b}$, which appear in the definition of $\bar{\psi}$. Three additional equations must then be imposed together with Eq. (3),

$$\psi_\mathrm{a} = \psi(P_\mathrm{a}) \tag{5}$$

$$\psi_\mathrm{b} = \psi(P_\mathrm{b}) \tag{6}$$

$$\int_{\Omega_\mathrm{p}} J_{\mathrm{p}\varphi}\,\mathrm{d}\Omega = I_\mathrm{p} \tag{7}$$

where $P_\mathrm{a}$ is the position of the magnetic axis (i.e. the plasma point where $\psi$ is a maximum), $P_\mathrm{b}$ the position of a boundary point (i.e. the limiter point or the X point) and $\Omega_\mathrm{p}$ the poloidal cross-section of the plasma region $V_\mathrm{p}$.

Equations (3), (5), (6) and (7) provide a direct link between $\psi$ and $J_\varphi$. Once all the currents $\boldsymbol{x} = (I_1, ..., I_n, I_\mathrm{p})$ and the plasma profile parameters $\boldsymbol{s} = (\alpha_m, \alpha_n, \beta_0)$ are given, the flux distribution and $\boldsymbol{q} = (\psi_\mathrm{a}, \psi_\mathrm{b}, \lambda)$ can be determined. Thus, $\boldsymbol{x}$ and $\boldsymbol{s}$ might be regarded as the state variables. However, as described in Section 2.1, we assume $\boldsymbol{s}$ to play the role of a disturbance and suppose it to be prescribed as a function of time. Therefore, $n + 1$ equations must be written in order to determine the time evolution of all the currents (including $I_\mathrm{p}$).

From Ohm's law

$$\boldsymbol{E} + \boldsymbol{E}_\mathrm{ext} = \eta \boldsymbol{J} \tag{8}$$

where $\boldsymbol{E}$ is the electric field, $\eta$ the electric resistivity and $\boldsymbol{E}_\mathrm{ext}$ the impressed field, we can obtain $n$ independent equations [19–21],

$$2\pi \int_{\Omega_\mathrm{PF}} J_{i\varphi}\dot{\psi}\,\mathrm{d}\Omega + \sum_{k=1}^{n} M_{ik}^\mathrm{pol}\dot{I}_k + \sum_{k=1}^{n} R_{ik} I_k = u_i \tag{9}$$

where $i = 1, ..., n$, $\Omega_\mathrm{PF}$ is the poloidal cross-section of the whole conducting region $V_\mathrm{PF}$, the dots stand for time derivatives, $\mathbf{R}$ is the resistance matrix defined by

$$R_{ik} = \int_{V_\mathrm{PF}} \eta \boldsymbol{J}_i \cdot \boldsymbol{J}_k\,\mathrm{d}V$$

$M_{ik}^\mathrm{pol}$ the contribution to the mutual inductance between the $i$th and the $k$th circuits due to the poloidal and non-axisymmetric currents and $\boldsymbol{u}$ the set of applied voltages defined by

$$u_i = \int_{V_\mathrm{PF}} \boldsymbol{J}_i \cdot \boldsymbol{E}_\mathrm{ext}\,\mathrm{d}V.$$

The final equation, i.e. the additional equation for the plasma current, is

$$\int_{V_\mathrm{p}} \boldsymbol{J}_\mathrm{p} \cdot \boldsymbol{E}\,\mathrm{d}V + \int_{V_\mathrm{p}} \boldsymbol{J}_\mathrm{p} \cdot (\boldsymbol{v} \times \boldsymbol{B})\,\mathrm{d}V = \int_{V_\mathrm{p}} \boldsymbol{J}_\mathrm{p} \cdot \eta_\mathrm{p} \boldsymbol{J}_\mathrm{p}\,\mathrm{d}V \tag{10}$$

where $\eta_\mathrm{p}$ is the plasma resistivity tensor, $\boldsymbol{J}_\mathrm{p}$ the plasma current density (with both toroidal and poloidal components), $\boldsymbol{v}$ the macroscopic velocity and $\boldsymbol{B}$ the magnetic field.

This equation can be derived from Ohm's law inside the plasma,

$$\boldsymbol{E} + (\boldsymbol{v} \times \boldsymbol{B}) = \eta_\mathrm{p} \boldsymbol{J}_\mathrm{p} \tag{11}$$

by multiplying both sides by $\boldsymbol{J}_\mathrm{p}$ and integrating over the whole plasma volume.

### 2.3. Linearization

Let us suppose that the reference values of $\boldsymbol{x}$, $\boldsymbol{u}$ and $\boldsymbol{s}$ are perturbed by $\delta\boldsymbol{x}$, $\delta\boldsymbol{u}$ and $\delta\boldsymbol{s}$, respectively. In the following, the reference quantities are indicated with the subscript '0'. The corresponding first order variations $\delta\psi$ and $\delta\boldsymbol{q}$ are the solutions of

$$L\delta\psi = \delta J_\varphi \tag{12}$$

$$\delta\psi_\mathrm{a} = \delta\psi(P_\mathrm{a0}) \tag{13}$$

$$\delta\psi_\mathrm{b} = \delta\psi(P_\mathrm{b0}) \tag{14}$$

$$\int_{\Omega_\mathrm{p0}} \delta J_\varphi \,\mathrm{d}\Omega = \delta I_\mathrm{p} \tag{15}$$

where $\delta J_\varphi$ is given by

$$\delta J_\varphi = \frac{\partial J_{\mathrm{p}\varphi}}{\partial\psi}\,\delta\psi + \frac{\partial J_{\mathrm{p}\varphi}}{\partial\boldsymbol{q}}\,\delta\boldsymbol{q} + \frac{\partial J_{\mathrm{p}\varphi}}{\partial\boldsymbol{s}}\,\delta\boldsymbol{s} \tag{16}$$

inside the plasma and

$$\delta J_\varphi = \sum_{k=1}^{n} \delta I_k J_{k\varphi}(r,z) \tag{17}$$

elsewhere.

Equations (13) and (14) state that the first order variations of $\psi_\mathrm{a}$ and $\psi_\mathrm{b}$ are given by the corresponding variations of $\psi$ at the reference positions of the axis and boundary points, disregarding their displacements. In general, the first order variation at a point moving from $P_0$ to $P_0 + \delta P$ is given by

$$(\psi+\delta\psi)|_{P_0+\delta P} - \psi(P_0) = \delta\psi(P_0) + \nabla\psi(P_0)\cdot\delta P. \tag{18}$$

The additional term $\nabla\psi(P_0)\cdot\delta P$ vanishes for the magnetic axis because $\nabla\psi(P_\mathrm{a}) = 0$. The same holds for the boundary point for diverted configurations, since the magnetic field vanishes at the X point. In the limiter configuration, the contact point (i.e. the point at which the plasma touches the wall) has a non-zero magnetic field. However, in such cases the plasma is tangential to the first wall at the contact point, so that $\nabla\psi$ is normal to the wall. Therefore, the additional term is also zero in the limiter case, because a normal movement of the contact point is not allowed: it would correspond to a penetration into the wall or a detachment from the wall, which is excluded, as pointed out in Section 2.1. On the other hand, using the alternative assumption of frozen boundary flux, Eqs (13) and (14) would be replaced by $\delta\psi_\mathrm{a} = \delta\psi_\mathrm{b} = 0$.

Finally, in Eq. (15) we have neglected the surface term, since $\Omega_\mathrm{p0}$ stands for the unperturbed plasma surface. This is consistent with our expression for the current density, which vanishes on the plasma boundary.

Applying the same linearization procedure to Eq. (9), we obtain the perturbed circuit equations,

$$2\pi\int_{\Omega_\mathrm{PF}} J_{i\varphi}\delta\dot\psi\,\mathrm{d}\Omega + \sum_{k=1}^{n} M_{ik}^\mathrm{pol}\delta\dot I_k + \sum_{k=1}^{n} R_{ik}\delta I_k = \delta u_i \tag{19}$$

for $i = 1, ..., n$.

Using a similar procedure, linearization of Eq. (11) yields

$$\int_{V_\mathrm{p0}} \boldsymbol{J}_\mathrm{p0}\cdot\delta\boldsymbol{E}\,\mathrm{d}V + \int_{V_\mathrm{p0}} \boldsymbol{J}_\mathrm{p0}\cdot\delta(\boldsymbol{v}\times\boldsymbol{B})\,\mathrm{d}V = \int_{V_\mathrm{p0}} \boldsymbol{J}_\mathrm{p0}\cdot\eta_\mathrm{p}\delta\boldsymbol{J}_\mathrm{p}\,\mathrm{d}V. \tag{20}$$

Assuming that $\boldsymbol{v}_0 = \boldsymbol{0}$ and $\eta_\mathrm{p} = 0$, and taking into account the fact that the equilibrium implies $\boldsymbol{J}_\mathrm{p0}\times\boldsymbol{B}_0 = \nabla p_0$, Eq. (20) can be rewritten as

$$\int_{V_\mathrm{p0}} \delta\boldsymbol{E}\cdot\boldsymbol{J}_\mathrm{p0}\,\mathrm{d}V - \int_{V_\mathrm{p0}} \delta\boldsymbol{v}\cdot\boldsymbol{\nabla}p_0\,\mathrm{d}V = 0 \tag{21}$$

or, as described in Appendix A, in terms of the poloidal flux per radian,

$$\int_{V_\mathrm{p0}} \left(\frac{\delta\dot\psi}{\mu_0 r^2}\,f_0\,\frac{\mathrm{d}f_0}{\mathrm{d}\psi} + \frac{f_0 - f_\mathrm{B0}}{\mu_0 r^2}\,\delta\dot f\right)\mathrm{d}V = 0 \tag{22}$$

where $f_\mathrm{B}$ is the value of $f$ at the plasma boundary.

From Eqs (1) and (2), with $j = (1-\bar\psi^{\alpha_m})^{\alpha_n}$, we can obtain the following expression for $h = f^2$:

$$h = f^2 = f_\mathrm{B}^2 + \lambda(1-\beta_0)R_0(\psi_\mathrm{b}-\psi_\mathrm{a})\int_1^{\bar\psi}(1-\chi^{\alpha_m})^{\alpha_n}\,\mathrm{d}\chi = h(\psi,\boldsymbol{q},\boldsymbol{s}) \tag{23}$$

and, finally, arrive at the form of the linearized equation for the plasma current used in our model,

$$\int_{\Omega_\mathrm{p0}} \left[\frac{\delta\dot\psi}{r}\,\frac{\mathrm{d}h_0}{\mathrm{d}\psi} + \frac{f_0 - f_\mathrm{B0}}{f_0 r}\left(\frac{\partial h_0}{\partial\psi}\,\delta\dot\psi + \frac{\partial h_0}{\partial\boldsymbol{q}}\,\delta\dot{\boldsymbol{q}} + \frac{\partial h_0}{\partial\boldsymbol{s}}\,\delta\dot{\boldsymbol{s}}\right)\right]\mathrm{d}\Omega = 0. \tag{24}$$

Here we have implicitly assumed that $f_\mathrm{B}$ does not change in time. This is true if the current in the TF coil is constant and no poloidal current flows in the vessel. If this assumption is not met, additional equations have to be added for the poloidal circuits, and the contribution of the time derivative of $f_\mathrm{B}$ has to be included in Eq. (24).

### 2.4. Numerical solution

Section 2.3 indicates that we have to solve a system including the free boundary problem (12) to (15), the circuit equations (19) and, finally, Eq. (24), which can be regarded as an integral form of Ohm's law in the plasma.

For the solution of Eqs (12) to (15) we use the finite element method [8, 19–21]. The solution domain is partitioned into a number of subdomains (finite elements) over which the unknown is approximated by means of piecewise polynomial basis functions,

$$\delta\psi = \sum_{j=1}^{m} \delta\psi_j \varphi_j(r,z) \tag{25}$$

where the $\varphi_j$ are the basis functions associated with the $m$ nodes of the mesh.

Using Eq. (25) and applying the Galerkin method, Eqs (12) to (15) yield

$$\mathbf{M}\begin{pmatrix} \delta\boldsymbol{\psi} \\ \delta\boldsymbol{q} \end{pmatrix} = \mathbf{N}\begin{pmatrix} \delta\boldsymbol{x} \\ \delta\boldsymbol{s} \end{pmatrix} \tag{26}$$

where $\delta\boldsymbol{\psi} = (\delta\psi_1, ..., \delta\psi_m)$; expressions for $\mathbf{M}$, $\mathbf{N}$ and most of the matrices in this section are given in Appendix B to keep the main text easily readable.

Note that Eq. (26) establishes a direct link between $(\delta\boldsymbol{x}, \delta\boldsymbol{s})^{\mathrm{T}}$ and $(\delta\boldsymbol{\psi}, \delta\boldsymbol{q})^{\mathrm{T}}$,

$$\begin{pmatrix} \delta\boldsymbol{\psi} \\ \delta\boldsymbol{q} \end{pmatrix} = \mathbf{M}^{-1}\mathbf{N}\begin{pmatrix} \delta\boldsymbol{x} \\ \delta\boldsymbol{s} \end{pmatrix}. \tag{27}$$

Similarly, Eqs (19) and (24) yield $n+1$ scalar equations that, in the light of Eq. (25), can be rewritten as

$$\mathbf{T}\delta\dot{\boldsymbol{\psi}} + \begin{pmatrix} \mathbf{M}^{\mathrm{pol}} \\ \mathbf{0}^{\mathrm{T}} \end{pmatrix}\delta\dot{\boldsymbol{x}} + \mathbf{V}\delta\boldsymbol{x} - \delta\boldsymbol{u} = 0 \tag{28}$$

$$\boldsymbol{p}^{\mathrm{T}}\delta\dot{\boldsymbol{\psi}} + \boldsymbol{h}^{\mathrm{T}}\delta\dot{\boldsymbol{q}} + \boldsymbol{l}^{\mathrm{T}}\delta\dot{\boldsymbol{s}} = 0. \tag{29}$$

Eliminating $(\delta\boldsymbol{\psi}, \delta\boldsymbol{q})^{\mathrm{T}}$, by means of Eq. (27), from Eqs (28) and (29) we finally obtain the circuit equations in terms of modified inductance and resistance matrices,

$$\mathbf{L}^{*}\delta\dot{\boldsymbol{x}} + \mathbf{R}^{*}\delta\boldsymbol{x} = \delta\boldsymbol{u} - \mathbf{L}_{\mathrm{s}}^{*}\delta\dot{\boldsymbol{s}} \tag{30}$$

or in the state space form,

$$\delta\dot{\boldsymbol{x}} = \mathbf{A}\delta\boldsymbol{x} + \mathbf{B}\delta\boldsymbol{u} + \mathbf{E}_{\mathrm{s}}\delta\dot{\boldsymbol{s}}. \tag{31}$$

### 2.5. Output variables

The output variables of interest are the quantities defining the plasma position and shape (plasma current moments and gaps), the values of the field and fluxes at a number of points, and the plasma parameters $l_{\mathrm{i}}$ and $\beta_{\mathrm{p}}$.

The set of output parameters $\boldsymbol{y}$ is clearly a function of $\boldsymbol{\psi}$, $\boldsymbol{q}$ and $\boldsymbol{s}$. Linearizing this relationship we can write

$$\delta\boldsymbol{y} = \mathbf{K}\begin{pmatrix} \delta\boldsymbol{\psi} \\ \delta\boldsymbol{q} \\ \delta\boldsymbol{s} \end{pmatrix} \tag{32}$$

and, using Eq. (27), we finally obtain

$$\delta\boldsymbol{y} = \mathbf{C}\delta\boldsymbol{x} + \mathbf{D}\delta\boldsymbol{u} + \mathbf{F}_{\mathrm{s}}\delta\boldsymbol{s} \tag{33}$$

which complete the state space equations.

The methodology for obtaining the $\mathbf{K}$ matrix is now illustrated for the above mentioned parameters.

#### 2.5.1. Gaps

Let $P_{\mathrm{p}}$ be the closest point on the plasma boundary intersected by the direction $\boldsymbol{n}$ normal to the wall at $P_{\mathrm{g}}$. The first order variation of the gap amplitude $\delta g$ around its nominal value is given by

$$\delta g = \frac{\delta\psi(P_{\mathrm{p0}}) - \delta\psi_{\mathrm{b}}}{\dfrac{\partial\psi_0}{\partial n}(P_{\mathrm{p0}})} \tag{34}$$

where $P_{\mathrm{p0}}$ is, as usual, the reference position of $P_{\mathrm{p}}$.

#### 2.5.2. Internal inductance and poloidal beta

Assuming the following definitions:

$$l_{\mathrm{i}} = \frac{4W_{\mathrm{mpol}}}{\mu_0 R_0 I_{\mathrm{p}}^2}, \quad \beta_{\mathrm{p}} = \frac{W_{\mathrm{p}}}{W_{\mathrm{mpol}}} \tag{35a,b}$$

$$W_{\mathrm{mpol}} = \int_{V_{\mathrm{p}}} \frac{|\nabla\psi|^2}{2\mu_0 r^2}\,\mathrm{d}V, \quad W_{\mathrm{p}} = \int_{V_{\mathrm{p}}} p\,\mathrm{d}V \tag{35c,d}$$

we have to calculate the first-order variations of $W_{\mathrm{mpol}}$ and $W_{\mathrm{p}}$.

Since the pressure $p$ vanishes on the plasma boundary, the first order variation of $W_{\mathrm{p}}$ is

$$\begin{aligned}\delta W_{\mathrm{p}} &= \int_{V_{\mathrm{p0}}} \delta p\,\mathrm{d}V \\ &= \int_{V_{\mathrm{p0}}} \left(\frac{\partial p}{\partial\psi}\,\delta\psi + \frac{\partial p}{\partial\boldsymbol{q}}\,\delta\boldsymbol{q} + \frac{\partial p}{\partial\boldsymbol{s}}\,\delta\boldsymbol{s}\right)\mathrm{d}V\end{aligned} \tag{36}$$

where the derivatives of $p$ can easily be calculated once the derivatives of $h$ are known, since Eqs (1), (2) and (23) yield

$$p = \frac{(h - f_{\mathrm{B}}^2)}{2\mu_0 R_0^2} \frac{\beta_0}{1 - \beta_0}. \tag{37}$$

To calculate the first order variation of $W_{\mathrm{mpol}}$, we adopt the equivalent expression

$$W_{\mathrm{mpol}} = \pi \int_{\Omega_{\mathrm{p}}} J_{\mathrm{p}\varphi}(\psi - \psi_{\mathrm{b}})\, \mathrm{d}\Omega \tag{38}$$

in which the integrand vanishes on the plasma boundary, and hence the variation can be calculated as in (36).

#### 2.5.3. Plasma current moments

The usual definitions of the plasma current centroid position are used,

$$z_{\mathrm{p}} I_{\mathrm{p}} = \int_{\Omega_{\mathrm{p}}} z J_{\mathrm{p}\varphi}\, \mathrm{d}\Omega \tag{39a}$$

$$r_{\mathrm{p}}^2 I_{\mathrm{p}} = \int_{\Omega_{\mathrm{p}}} r^2 J_{\mathrm{p}\varphi}\, \mathrm{d}\Omega \tag{39b}$$

so that their variations are simply

$$\delta(z_{\mathrm{p}} I_{\mathrm{p}}) = \int_{\Omega_{\mathrm{p0}}} z \delta J_{\mathrm{p}\varphi}\, \mathrm{d}\Omega \tag{40a}$$

$$\delta(r_{\mathrm{p}}^2 I_{\mathrm{p}}) = \int_{\Omega_{\mathrm{p0}}} r^2 \delta J_{\mathrm{p}\varphi}\, \mathrm{d}\Omega. \tag{40b}$$

#### 2.5.4. Field and flux measurements

The $\mathbf{K}$ matrix contains only the terms related to $\delta\boldsymbol{\psi}$. The matrix coefficients are directly linked to the values and the gradients of the shape functions at the measurement points for fluxes and fields, respectively.

### 2.6. Comments and discussion

First of all, it is worth noticing that, assuming $\eta_{\mathrm{p}} = 0$, the plasma equation yields a static link between the plasma current and the coil currents. In other words, at each instant the plasma current can be expressed as a linear combination of the coil currents.

Eliminating $I_{\mathrm{p}}$ from the set of unknowns, Eq. (30) can be put in the form

$$\mathbf{L}_{\mathrm{r}}^* \delta\dot{\boldsymbol{I}} + \mathbf{R}_{\mathrm{r}}^* \delta\boldsymbol{I} = \delta\boldsymbol{u}_{\mathrm{r}} - \mathbf{L}_{\mathrm{sr}}^* \delta\dot{\boldsymbol{s}} \tag{41}$$

where $\mathbf{L}_{\mathrm{r}}^*$ is the reduced inductance matrix, $\mathbf{R}_{\mathrm{r}}^*$ the reduced resistance matrix, $\delta\boldsymbol{u}_{\mathrm{r}}$ the set of voltages applied to the circuits and $\mathbf{L}_{\mathrm{sr}}^*$ the linearized mapping between the disturbances and fluxes linked with the circuits. The reduced matrix $\mathbf{L}_{\mathrm{r}}^*$ is not symmetric; this means that the global electromagnetic system is not conservative. Indeed, it is not true in general that the overall magnetic energy content remains unchanged during a cyclic transformation. This is due both to the exchange between magnetic energy and pressure energy allowed by Eq. (24) and to our assumption about the boundary and axis fluxes. Indeed, this assumption allows, for instance, instantaneous dissipation, owing to the instantaneous decay of the poloidal currents flowing in the first wall. Conversely, assuming frozen boundary and axis fluxes there is energy conservation, and, as a consequence, $\mathbf{L}_{\mathrm{r}}^*$ is nearly symmetric. The discrepancies from symmetry are only due to the other forms of energy involved. We checked that for a force-free configuration the symmetry is almost perfect in the frozen flux case.

As a particular case, we consider the TCV tokamak [1], which is well suited for validating the model, owing to its wide variety of coils and the reliability of the many magnetic measurements available. The reference configuration is shown in Fig. 1 (shot 11611); we have 18 active circuits and 56 axisymmetric passive conductors simulating the electromagnetic behaviour of the vacuum vessel.

Figure 2 shows that $\mathbf{L}_{\mathrm{r}}^*$ is indeed nearly symmetric using the frozen boundary flux assumption. In addition, with the outermost closed surface flux assumption, there can be a sharp discontinuity in the plasma behaviour in the case of a transition between a limiter and a diverted configuration, which does

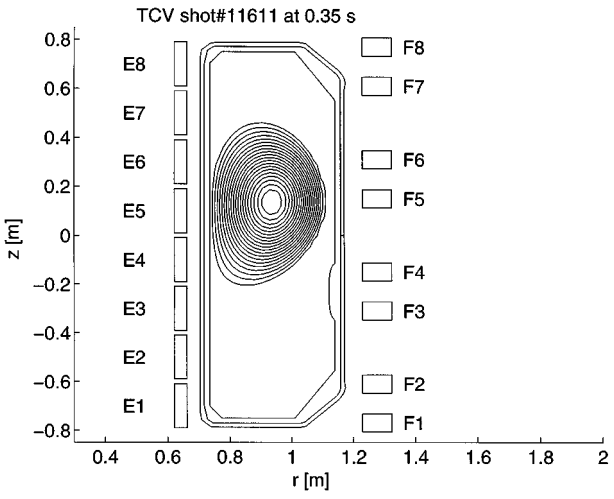


FIG. 1. TCV limiter configuration (shot 11611: $I_{\mathrm{p}} = 200$ kA, $\beta_{\mathrm{p}} = 0.40$, $l_{\mathrm{i}} = 1.13$).

**Table I. Effects of the Two Assumptions about Boundary Fluxes during the Transition Between a Limiter ($\alpha = 0.4$) and a Divertor ($\alpha = 0.5$) Configuration on Various $\mathbf{L}^*$ and $\mathbf{C}$ Elements**
(The plasma configuration is TVC shot 11611 presented in Section 4.2.)

| | Frozen boundary flux | | Outermost closed line | |
|---|---|---|---|---|
| | $\alpha = 0.4$ | $\alpha = 0.5$ | $\alpha = 0.4$ | $\alpha = 0.5$ |
| $L^*(75, 8)$ | $-9.2248 \times 10^{-8}$ | $-9.2609 \times 10^{-8}$ | $7.5793 \times 10^{-7}$ | $3.1801 \times 10^{-7}$ |
| $L^*(9, 16)$ | $-9.2225 \times 10^{-5}$ | $-8.9460 \times 10^{-5}$ | $-4.2385 \times 10^{-6}$ | $-2.3161 \times 10^{-6}$ |
| $C(24, 7)$ | $-4.7274 \times 10^{-5}$ | $-4.7236 \times 10^{-5}$ | $1.4579 \times 10^{-5}$ | $-3.1021 \times 10^{-5}$ |

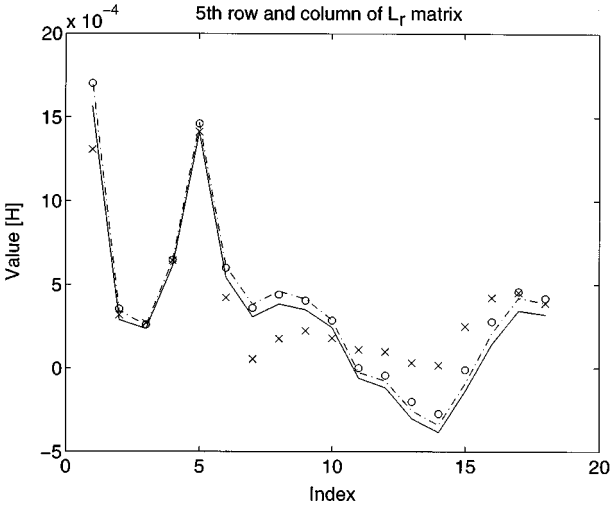


FIG. 2. Comparison between rows and columns of the $\mathbf{L}_r^*$ matrix for the plasma configuration shown in Fig. 1: the column (solid curve) and row (crosses) based on the outermost closed surface flux assumption versus the column (chain curve) and row (circles) based on the frozen boundary flux assumption. The first 18 circuits correspond to the active coils, the fifth one of which is E3.

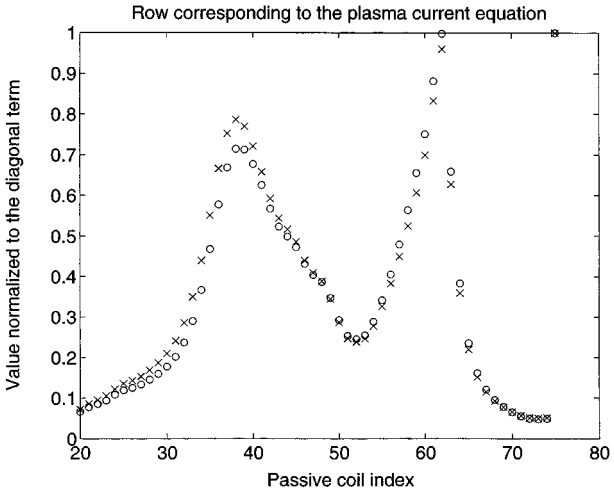


FIG. 3. Comparison between the modified inductance matrices based on different assumptions: circles, integral form of Ohm's law (24); crosses, average flux conservation (42). The reference configuration is shown in Fig. 1.

not occur when adopting the frozen boundary flux assumption (Table I). In any case, as stated in Section 2.1, we take the outermost closed surface flux assumption as the reference, because the main application of the plasma response model is to closed loop control, which is characterized by a rather long timescale.

Moreover, it must be stressed that the plasma equation (24) does not take into account Joule dissipation. Supposing that no energy interaction between the poloidal and the toroidal field takes place, and disregarding any pressure contribution, the linearized plasma equation becomes

$$\int_{\Omega_{p0}} J_{p\varphi 0} \delta\dot{\psi} \, d\Omega = 0. \tag{42}$$

This assumption was at the basis of the first, simplified version of the CREATE-L model used in Ref. [13], which is equivalent to the one presented here, based on Eq. (24), for low-$\beta$, high aspect ratio plasmas. Indeed, the $\mathbf{L}^*$ matrix is the same for both models, except for the last row, corresponding to the plasma equation. Figure 3 shows the two last rows of $\mathbf{L}^*$ from the two linearized models. In this case, the discrepancy is not significant, since the difference in the growth rates predicted by the two models is less than 0.1%, and the maximum difference between the eigenvalues of the corresponding $\mathbf{A}$ matrices is less than 2%.

Finally, it is worth making some comments about the treatment of the disturbances. Since we want to deal with disturbances in terms of $\boldsymbol{w} = (\beta_p, l_i)^T$ rather than in terms of $\boldsymbol{s} = (\alpha_m, \alpha_n, \beta_0)^T$, we express $\boldsymbol{s}$ as a static linear function of $\boldsymbol{w}$. As $\boldsymbol{w}$ is a

subset of $\boldsymbol{y}$, this link can be obtained from Eq. (33) by neglecting the contributions of $\delta\boldsymbol{x}$ and $\delta\boldsymbol{u}$, and pseudo-inverting the corresponding rows of $\boldsymbol{F}_\mathrm{s}$. The circuit equations can therefore be rewritten as

$$\mathbf{L}^*\delta\dot{\boldsymbol{x}} + \mathbf{R}^*\delta\boldsymbol{x} = \delta\boldsymbol{u} - \mathbf{L}^*_\mathrm{w}\delta\dot{\boldsymbol{w}} \tag{43}$$

whereas the state space form of the CREATE-L model becomes

$$\delta\dot{\boldsymbol{x}} = \mathbf{A}\delta\boldsymbol{x} + \mathbf{B}\delta\boldsymbol{u} + \mathbf{E}\delta\dot{\boldsymbol{w}} \tag{44}$$

$$\delta\boldsymbol{y} = \mathbf{C}\delta\boldsymbol{x} + \mathbf{D}\delta\boldsymbol{u} + \mathbf{F}\delta\boldsymbol{w}. \tag{45}$$

In previous versions of the CREATE-L model the **F** matrix was calculated using a finite difference approach on the results of a non-linear evolution corresponding to canonical disturbances [13]. Using the derivatives, as is done here, the results are not significantly different (Fig. 4).

The **E** matrix was also previously calculated using finite differences, calculating the 'jump' of the state variables in the presence of step-like drops of $\beta_\mathrm{p}$ and $l_\mathrm{i}$, using flux conservation in the circuits and an a priori assumption about the jump of the plasma current (for instance, the conservation of $l_\mathrm{i}I_\mathrm{p}^2$ [22]). In the present version, the **E** matrix is calculated assuming Eq. (24) to be valid even when $\boldsymbol{w}$ jumps. This can lead to perceptible, but not dramatic, differences between the **E** matrices obtained with the two different versions (Fig. 5).

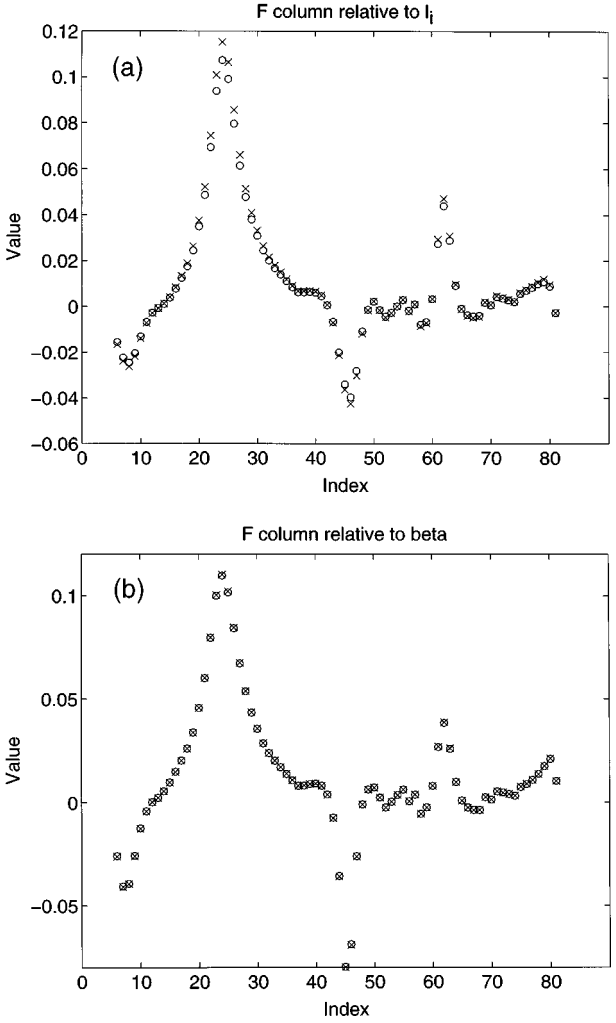


FIG. 4. **F** matrix for the reference configuration shown in Fig. 1, computed using derivatives (circles) or the finite difference approximation (crosses): columns corresponding to (a) $l_\mathrm{i}$ and (b) $\beta_\mathrm{p}$.

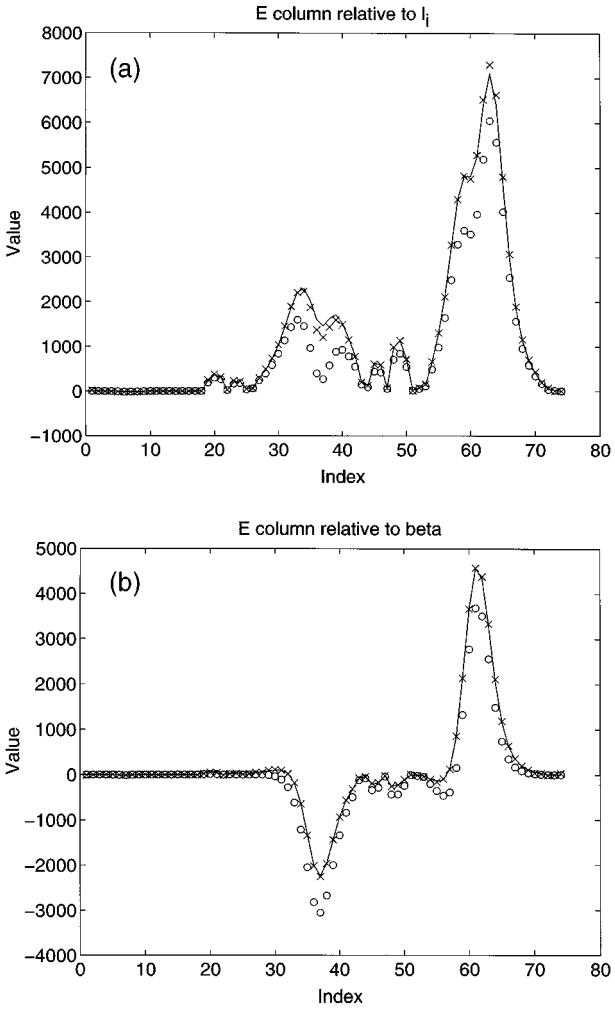


FIG. 5. **E** matrix for the reference configuration shown in Fig. 1: columns corresponding to (a) $l_\mathrm{i}$ and (b) $\beta_\mathrm{p}$. The crosses denote the values computed using the finite difference approximation with the $\Delta(l_\mathrm{i}I_\mathrm{p}^2) = 0$ assumption; the solid curves refer to the calculations using derivatives together with the $\Delta(l_\mathrm{i}I_\mathrm{p}^2) = 0$ assumption; the circles indicate the values obtained using derivatives together with Eq. (24).

Equation (24) is probably not valid, even in the presence of internal disturbances, when fast minor disruptions occur. As stated in Ref. [15], the simple model presented in this article is well suited for describing the electromagnetic interaction between plasma and surrounding currents, but is not directly able to determine the internal diffusion and transport phenomena. For this reason, it might be worthwhile to slightly modify the $\mathbf{E}$ matrix. This can be done by acting on the coefficients of the $\mathbf{L}_{\mathrm{w}}^{*}$ matrix corresponding to the disturbances. In this way, it is possible to have an instantaneous change of $I_{\mathrm{p}}$ due to a jump in $\boldsymbol{w}$, which is consistent with experimental observations, predictions of transport codes, or other assumptions. Figure 5 shows a comparison between the results obtained with Eq. (24) and those with the alternative assumption $\Delta(l_{\mathrm{i}} I_{\mathrm{p}}^{2}) = 0$.

## 3. MODEL VALIDATION

### 3.1. Rationale

One of the main objectives of this work is to verify that the linearized model is reliable for the design of the control system. Therefore, we tried to assess the following points:

(a) The linearized model is properly implemented.
(b) The amplitudes of the disturbances and control currents that are expected allow us to assume that the system remains in its linearity range without significant approximation errors.
(c) The assumptions on which the plasma model is derived are correct.

The first two points can be assessed by comparing the results of the linear model with those of a non-linear code that solves exactly the same equilibrium and circuit equations, i.e. the corresponding non-linear model. The PROTEUS code [19–21] is well suited for this purpose. The third point is a critical issue. Once the first two points are satisfied, the correctness of the assumptions can be verified by comparing the results with those of different non-linear models and with experimental data.

### 3.2. Comparison of the linear and the corresponding non-linear model

We assessed the matrices obtained with the CREATE-L model and the associated code via a comparison with the PROTEUS code. Of course, this validation, mainly addressed towards the determination of the linearity range, did not challenge the model significantly.

To check the correctness of $\mathbf{A}$, $\mathbf{B}$, $\mathbf{C}$ and $\mathbf{D}$, assuming that the resistance matrix is correctly computed, we tested only the $\mathbf{L}^{*}$ matrix and the $\mathbf{C}$ matrix, since $\mathbf{D} = \mathbf{0}$, $\mathbf{A} = -(\mathbf{L}^{*})^{-1}\mathbf{R}^{*}$ and $\mathbf{B} = (\mathbf{L}^{*})^{-1}$. The test cases were several configurations of the TCV and ITER tokamaks. The data reported in this section for mere illustrative purposes refer to the TCV limiter configuration illustrated in Fig. 1. A similar analysis is reported in Ref. [22] for the ITER TAC-8 X point configuration at the end of its burn using the linearized model based on Eq. (42).

We computed the values of gaps, fields and fluxes as functions of the E3 coil current, using both PROTEUS and the linearized CREATE-L model. This coil current was parametrized according to the law $I_{\mathrm{E3}}(\alpha) = (28.1 + 27.3\alpha)$ kA. The situation $\alpha = 0$ corresponds to the original TCV limiter configuration, whereas $\alpha = 1$ corresponds to a fictitious diverted configuration; the transition occurs between $\alpha = 0.4$ and $\alpha = 0.5$. The plasma current density profile, but not the total plasma current, was kept fixed in both linearized and non-linear calculations.

Figure 6 shows a comparison between the linear and the non-linear fluxes linked with one circuit. This figure suggests that the $\mathbf{L}^{*}$ matrix is correctly computed and that the linearized model works well for current changes that are a considerable fraction of the plasma current, provided that the plasma does not leave the wall. In that case, the plasma behaviour may

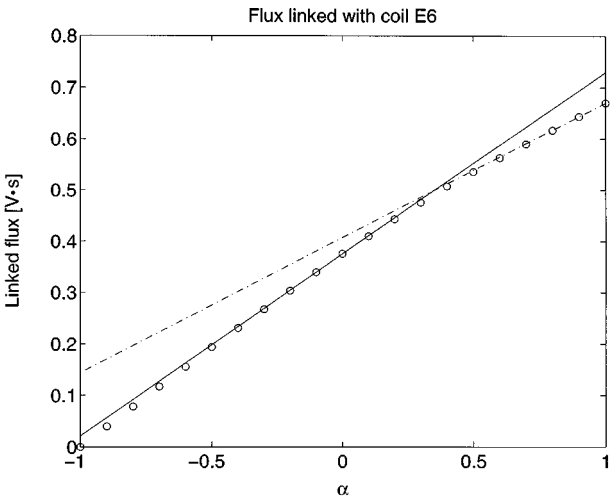


FIG. 6. Flux linked with coil E6 as a function of the E3 current variation in the configuration shown in Fig. 1: $I_{\mathrm{E3}}(\alpha) = (28.1 + 27.3\alpha)$ kA. The circles indicate the predictions of the non-linear model, whereas the solid line and the chain line indicate the predictions of the linearized models corresponding to $\alpha = 0$ (reference limiter configuration) and $\alpha = 1$ (diverted configuration), respectively.

change dramatically from limiter to diverted configurations, unless the frozen boundary flux model is assumed.

The previous statement is also valid for the **C** matrix. The results of the linearized and non-linear models are in very good agreement (Fig. 7).

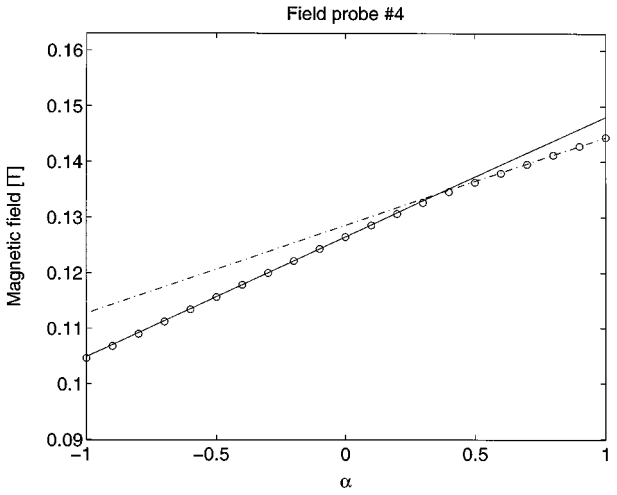


FIG. 7. Poloidal flux at a measurement point ($r$ = 0.606 m, $z$ = 0.345 m) as a function of the E3 current variation in the configuration shown in Fig. 1: $I_{E3}(\alpha) = 28.1+27.3\alpha$ kA. The circles indicate the predictions of the non-linear model, whereas the solid line and the chain line indicate the predictions of the linearized models corresponding to $\alpha = 0$ (reference limiter configuration shown in Fig. 1) and $\alpha = 1$ (diverted configuration), respectively.

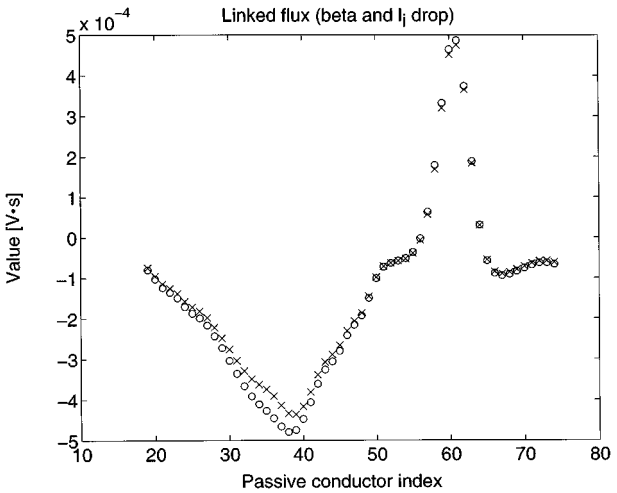


FIG. 8. Variation of the flux linked with the vessel conductors due to a combined $\beta_p$ and $l_i$ drop. The circles denote the linearized model predictions, whereas the crosses indicate the actual non-linear variations. The reference configuration is shown in Fig. 1.

We also tested the **E** and **F** matrices. With this analysis we verified that the effects of $l_i$ and $\beta_p$ disturbances are by far dominant with respect to those induced by the change of other parameters such as the safety factor at the magnetic axis [15, 22]. Figures 8 and 9 show a comparison between the non-linear behaviour and the results predicted by the CREATE-L model in the case of a combined $l_i$ and $\beta_p$ step ($\Delta\beta_p = -0.020$, $\Delta l_i = 0.017$).

The results of this analysis show that the plasma behaviour is not far from being linear and, consequently, the predictions of the linearized CREATE-L model are reliable even for large amplitudes of the disturbances and large current changes, provided that there is no transition between limiter and diverted configurations.

### 3.3. Comparison with different models

We also compared the results of the CREATE-L model with those provided by alternative linear and non-linear models. These comparisons were made with the CREATE-L version based on plasma current equation (42) and the derivation of the **E** and **F** matrices described in Ref. [13]. These tests are still significant in view of the results illustrated in Section 2.5.

First of all we compared the CREATE-L model with the simple rigid displacement plasma model, which is widely used for the analysis and stabilization of the vertical motion of the plasma. The plasma

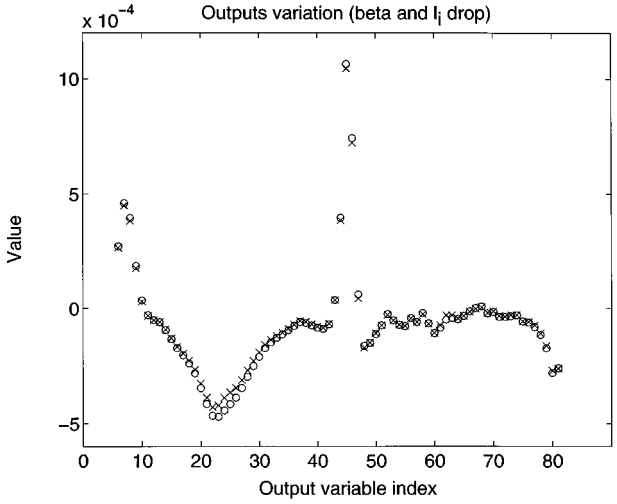


FIG. 9. Variations of some of the output variables (flux and field measurements) due to a combined $\beta_p$ and $l_i$ drop. The circles denote the linearized model predictions, whereas the crosses indicate the actual non-linear variations. The reference configuration is shown in Fig. 1.

configuration analysed refers to TCV shot 10396, which corresponds to an up–down symmetric limiter configuration. The growth rate of the vertical instability provided by the CREATE-L model is around 400 $s^{-1}$, whereas the value provided by the rigid displacement model is around 500 $s^{-1}$. This is consistent with the analysis of the growth mode, which is characterized by a vertical velocity varying in a range of about 20% around its average value. With an up–down symmetric equilibrium configuration and an antisymmetric excitation, the basic assumptions of the rigid plasma model are essentially satisfied [1]. We have therefore compared the open loop input–output behaviour of the system assuming as the input quantity an antisymmetric excitation of PF coils E1 and E8 and as the output quantity the plasma current moment $z_p I_p$. The corresponding Bode diagrams are illustrated in Fig. 10. A thorough comparison in the closed loop situation is reported in Ref. [23].

In Ref. [24], the CREATE-L model predictions were compared with the CORSICA model [25] of an ITER configuration. The two models differ both in the plasma response to external coil inputs and in the treatment of the fast internal plasma disturbances. Indeed, for what concerns the coil inputs, the CORSICA model conserves the integral over the plasma cross-section of the product of the flux and the current density. The effects of changes in $l_i$ and $\beta_p$ are taken into account in the CORSICA model by conserving the helicity and the $q$ profile, respectively. In this case, the growth rates of the vertical instability

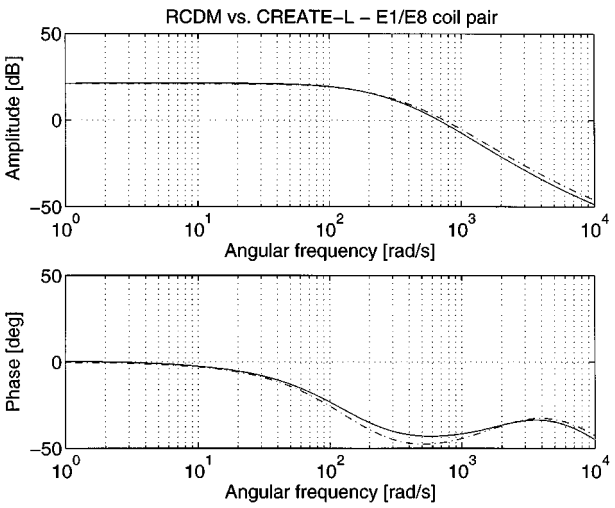


FIG. 10. Bode diagrams of the E1, E8 coil pair voltage to $z_p I_p$ transfer functions as given by the CREATE-L model (solid curves) and by the RCDM model (chain curves) for TCV shot 10396.

are 0.89 $s^{-1}$ (CREATE-L) and 0.82 $s^{-1}$ (CORSICA). A thorough analysis of the input–output behaviours was made, assuming as input quantities the PF coil voltages, and taking the PF coil currents, plasma current and plasma–wall distance as outputs. The comparison of the open loop dynamic responses showed a satisfactory agreement when looking at the Bode diagrams in the range of frequencies of interest [24]. Two distinct controllers were designed on the basis of the two different models. The closed loop analyses showed that each controller worked properly in both plant models, in spite of different assumptions. It is well known that a control system must be sufficiently robust with respect to the model uncertainties. The discrepancies between different models can be used to provide an indication of the model uncertainty to be considered when designing a robust controller. The results presented in Ref. [24] demonstrate that it is possible to design a controller that is robust to the difference between the CREATE-L and the CORSICA open loop model.

Finally, the CREATE-L model was compared with various non-linear models. Section 3.2 reported the comparison with the non-linear PROTEUS model from which the CREATE-L model is derived. This analysis was carried out only for the reasons explained in Section 3.1. Additional, more significant, tests were carried out using the non-linear codes TSC [7] and MAXFEA [26]. Open loop simulations were performed to see the plasma response to square pulse voltage injections in the PF coil voltages and to step-like $l_i$ and $\beta_p$ disturbances for ITER configurations. The details of the comparisons are given in Refs [27, 28]. Here, we simply summarize the main results of these analyses. In both cases, there is an excellent agreement between the CREATE-L model and the non-linear model in the case of PF coil voltage inputs. The agreement is less good, but still satisfactory, in the case of plasma disturbances, mainly because of the different assumptions about the plasma behaviour in the presence of minor disruptions, which are not self-consistently treated in CREATE-L [27]. Additional studies on the modelling of plasma disturbances are therefore needed. However, the overall agreement supports the use of the linearized model in the design of controllers.

### 3.4. Comparison with experimental results

There is a great interest in the validity of the models with respect to the response of a tokamak plasma to changes in the surrounding currents.

Several plasma models with different physical assumptions are currently being used for the design of future tokamaks. It was therefore considered essential to carry out a comprehensive validation of the CREATE-L model on an existing tokamak.

A work programme was then started in co-operation with CRPP, Lausanne, aimed at an extensive comparison between the real plasma response and the CREATE-L linearized model of the TCV tokamak. The results of the comparison made with the version based on plasma current equation (42) are presented in detail elsewhere [23]. Here, we simply summarize the main results:

(a) Firstly, it was necessary to perform closed loop experiments because of the vertical instability of the elongated plasmas under consideration. Therefore, a model of the TCV control system had to be added to the simulation.

(b) Secondly, the tests were carried out on the resistive time-scale, on which the system necessarily experiences a drift due to the resistive flux consumption. For this reason, in the comparison a least squares straight line fit was removed from both the experimental data and the simulation responses to remove their offsets and linear drifts [23].

(c) Thirdly, no modifications to the CREATE-L models were made to fit the experimental data.

(d) Finally, only the response to PF coil voltage injections was studied, so restraining the validation to the **A**, **B**, **C** and **D** matrices. The analyses of the plasma response to the disturbances, i.e. the tests on **E** and **F** matrices, have yet to be done.

The resulting excellent agreement reported in Ref. [23] shows that the physical assumptions are appropriate for control purposes.

## 4. CONCLUSIONS

In this article we have presented the CREATE-L linear plasma response model. It reproduces the features of the plasma behavior that are relevant to the control of current, position and shape. Since it is a linear model, it is very attractive both from the analysis point of view, since a simulation is not computationally intensive, and from the controller design point of view, since all the established control techniques can be applied. Moreover, it is a completely a priori model, in the sense that it does not need any tuning in order to increase the agreement with experiments or other models.

The main assumption which CREATE-L relies on is that a plasma can be characterized by means of a small set of parameters. Doing so, we are able to obtain a linearized model in which the state variables are the coil and plasma currents, and in which the profile quantities are seen as disturbances. The plasma current variation due to sudden $\beta_p$ or $l_i$ drops can be chosen so as to fit the experimental observations or the predictions of the transport codes, without taking them into account self-consistently. The flux on the boundary can be assumed to be either frozen (fast phenomena) or equal to the flux variation in the unperturbed boundary point (slow phenomena). This choice has an effect on the plasma response and on the energy balance of the system.

The comparison with experimental results and non-linear simulations suggests that the effects of the plasma on the overall closed loop system are properly modelled. The comparison with several non-linear codes indicates that the behaviour of the main plasma figures are satisfactorily modelled even in the open loop situation, and that the linearity range is wide enough in most cases.

The models resulting from the different physical assumptions do not seem to be dramatically different. They are likely to give rise to very similar closed loop models. The only critical situation seems to be the transition between limiter and diverted configurations. In this case, an effort should be made to understand in depth the physics of the phenomenon, to see which is the correct assumption to make.

These considerations indicate that the CREATE-L model is an effective tool for the design of the control system in existing and future tokamaks.

## Appendix A

In this Appendix, we illustrate the derivation of Eq. (22). Assuming $\eta_p = 0$, the toroidal projection of Eq. (11) yields

$$\delta\dot{\psi} = -\delta\boldsymbol{v}\cdot\boldsymbol{\nabla}\psi. \tag{46}$$

Then, using Eq. (1) and the fact that

$$\boldsymbol{\nabla}p = \frac{\mathrm{d}p}{\mathrm{d}\psi}\,\boldsymbol{\nabla}\psi \tag{47}$$

Eq. (21) becomes

$$-\int_{V_{p0}} \frac{\delta\dot{\psi}}{\mu_0 r^2}\, f_0\, \frac{\mathrm{d}f_0}{\mathrm{d}\psi}\,\mathrm{d}V + \int_{V_{p0}} \delta\boldsymbol{E}_{pol}\cdot\boldsymbol{J}_{pol0}\,\mathrm{d}V = 0 \tag{48}$$

where the suffix 'pol' indicates the poloidal quantities. Poynting's theorem yields

$$\int_{V_{\rm p0}} \delta \boldsymbol{E}_{\rm pol} \cdot \boldsymbol{J}_{\rm pol0}\,{\rm d}V = \int_{V_{\rm p0}} \delta \boldsymbol{E}_{\rm pol} \cdot \boldsymbol{\nabla} \times \boldsymbol{H}_{\varphi 0}\,{\rm d}V$$
$$= -\int_{V_{\rm p0}} \boldsymbol{\nabla} \cdot (\delta \boldsymbol{E}_{\rm pol} \times \boldsymbol{H}_{\varphi 0})\,{\rm d}V$$
$$+ \int_{V_{\rm p0}} \boldsymbol{\nabla} \times \delta \boldsymbol{E}_{\rm pol} \cdot \boldsymbol{H}_{\varphi 0}\,{\rm d}V$$
$$= -\int_{\partial V_{\rm p0}} (\delta \boldsymbol{E}_{\rm pol} \times \boldsymbol{H}_{\varphi 0}) \cdot \hat{\boldsymbol{n}}\,{\rm d}S$$
$$- \int_{V_{\rm p0}} \frac{\partial \delta \boldsymbol{B}_{\varphi}}{\partial t} \cdot \boldsymbol{H}_{\varphi 0}\,{\rm d}V \qquad (49)$$

where

$$\int_{\partial V_{\rm p0}} (\delta \boldsymbol{E}_{\rm pol} \times \boldsymbol{H}_{\varphi 0}) \cdot \hat{\boldsymbol{n}}\,{\rm d}S$$
$$= -\frac{2\pi f_{\rm B0}}{\mu_0} \int_{\Omega_{\rm p0}} \frac{\partial \delta B_{\varphi}}{\partial t}\,{\rm d}\Omega$$
$$= -\int_{V_{\rm p0}} \frac{\partial \delta B_{\varphi}}{\partial t} \frac{f_{\rm B0}}{\mu_0 r}\,{\rm d}V. \qquad (50)$$

Equation (22) is obtained from Eq. (48) taking into account Eqs (49) and (50).

## Appendix B

In this Appendix we give expressions for most of the matrices described in Section 2. In Eq. (26) we define

$$\mathbf{M} = \begin{pmatrix} \mathbf{M}_{11} & \mathbf{M}_{12} \\ \mathbf{M}_{21} & \mathbf{M}_{22} \end{pmatrix} \qquad (51a)$$

$$\mathbf{N} = \begin{pmatrix} \mathbf{N}_{11} & \mathbf{N}_{12} \\ \mathbf{N}_{21} & \mathbf{N}_{22} \end{pmatrix} \qquad (51b)$$

where, taking into account Eqs (3) to (7), we have

$$\mathbf{M}_{11}(i,j) = \int_{\Omega_{\rm p0}} \left( \frac{\boldsymbol{\nabla}\varphi_i \cdot \boldsymbol{\nabla}\varphi_j}{\mu r} - \varphi_i \varphi_j \frac{\partial J_{\rm p\varphi}}{\partial \psi} \right) {\rm d}\Omega \qquad (52)$$

with $1 \le i \le m$, $1 \le j \le m$,

$$\mathbf{M}_{12}(i,j) = -\int_{\Omega_{\rm p0}} \varphi_i \frac{\partial J_{\rm p\varphi}}{\partial q_j}\,{\rm d}\Omega \qquad (53)$$

with $1 \le i \le m$, $1 \le j \le 3$,

$$\mathbf{M}_{21}(1,j) = -\varphi_j(P_{\rm a0}) \qquad (54a)$$

$$\mathbf{M}_{21}(2,j) = -\varphi_j(P_{\rm b0}) \qquad (54b)$$

$$\mathbf{M}_{21}(3,j) = \int_{\Omega_{\rm p0}} \varphi_j \frac{\partial J_{\rm p\varphi}}{\partial \psi}\,{\rm d}\Omega \qquad (54c)$$

with $1 \le j \le m$

$$\mathbf{M}_{22} = \begin{pmatrix} 1 & 0 & 0 \\ 0 & 1 & 0 \\ t_1 & t_2 & t_3 \end{pmatrix}, \quad t_j = \int_{\Omega_{\rm p0}} \frac{\partial J_{\rm p\varphi}}{\partial q_j}\,{\rm d}\Omega \qquad (55)$$

with $1 \le j \le 3$,

$$\mathbf{N}_{11}(i,j) = \int_{\Omega_{\rm p0}} \varphi_i J_{j\varphi}\,{\rm d}\Omega, \quad j = 1, ..., n \qquad (56a)$$

$$\mathbf{N}_{11}(i,j) = 0, \quad j = n+1 \qquad (56b)$$

with $1 \le i \le m$

$$\mathbf{N}_{12}(i,j) = \int_{\Omega_{\rm p0}} \varphi_i \frac{\partial J_{\rm p\varphi}}{\partial s_j}\,{\rm d}\Omega \qquad (57)$$

with $1 \le i \le m$, $1 \le j \le 3$

$$\mathbf{N}_{21}(i,j) = 1, \quad i = 3, \quad j = n+1 \qquad (58a)$$

$$\mathbf{N}_{21}(i,j) = 0, \quad \text{otherwise} \qquad (58b)$$

$$\mathbf{N}_{22} = \begin{pmatrix} \partial \psi_{\rm a}/\partial \boldsymbol{s} \\ \partial \psi_{\rm b}/\partial \boldsymbol{s} \\ \boldsymbol{t}_4^{\rm T} \end{pmatrix} \qquad (59a)$$

and

$$\boldsymbol{t}_4^{\rm T} = -\int_{\Omega_{\rm p0}} \frac{\partial J_{\rm p\varphi}}{\partial \boldsymbol{s}}\,{\rm d}\Omega. \qquad (59b)$$

In Eq. (28) we have, from Eq. (19),

$$\mathbf{T}(j,i) = 2\pi \int_{\Omega_{\rm PF}} \varphi_i J_{j\varphi}\,{\rm d}\Omega \qquad (60)$$

with $1 \le i \le m$, $1 \le j \le n+1$, and

$$\mathbf{V}(i,j) = \mathbf{R}(i,j), \quad 1 \le j \le n \qquad (61a)$$

$$\mathbf{V}(i,j) = 0, \quad j = n+1 \qquad (61b)$$

with $1 \le i \le n+1$. In Eq. (29) we have, from Eq. (24),

$$\boldsymbol{p}^{\rm T}(i) = \int_{\Omega_{\rm p0}} \left(1 + \frac{f_0 - f_{\rm B0}}{f_0}\right) \frac{\varphi_i}{r} \frac{\partial h_0}{\partial \psi}\,{\rm d}\Omega \qquad (62)$$

with $1 \le i \le m$,

$$\boldsymbol{h}^{\rm T} = \int_{\Omega_{\rm p0}} \frac{f_0 - f_{\rm B0}}{r f_0} \frac{\partial h_0}{\partial \boldsymbol{q}}\,{\rm d}\Omega \qquad (63)$$

$$\boldsymbol{l}^{\rm T} = \int_{\Omega_{\rm p0}} \frac{f_0 - f_{\rm B0}}{r f_0} \frac{\partial h_0}{\partial \boldsymbol{s}}\,{\rm d}\Omega. \qquad (64)$$

Defining

$$\mathbf{G} = \mathbf{M}^{-1}\mathbf{N} = \begin{pmatrix} \mathbf{G}_{11} & \mathbf{G}_{12} \\ \mathbf{G}_{21} & \mathbf{G}_{22} \end{pmatrix} \tag{65}$$

we have in Eq. (30),

$$\mathbf{L}^* = \begin{pmatrix} \mathbf{T} \\ \boldsymbol{p}^{\mathrm{T}} \end{pmatrix}\mathbf{G}_{11} + \begin{pmatrix} \mathbf{0} \\ \boldsymbol{h}^{\mathrm{T}} \end{pmatrix}\mathbf{G}_{21} + \begin{pmatrix} \mathbf{M}^{\mathrm{pol}} \\ \mathbf{0}^{\mathrm{T}} \end{pmatrix} \tag{66}$$

$$\mathbf{R}^* = \begin{pmatrix} \mathbf{V} \\ \mathbf{0}^{\mathrm{T}} \end{pmatrix} \tag{67}$$

$$-\mathbf{L}_{\mathrm{s}}^* = \begin{pmatrix} \mathbf{T} \\ \boldsymbol{p}^{\mathrm{T}} \end{pmatrix}\mathbf{G}_{12} + \begin{pmatrix} \mathbf{0} \\ \boldsymbol{h}^{\mathrm{T}} \end{pmatrix}\mathbf{G}_{22} + \begin{pmatrix} \mathbf{0} \\ \boldsymbol{l}^{\mathrm{T}} \end{pmatrix} \tag{68}$$

and hence, in Eq. (31),

$$\mathbf{A} = -(\mathbf{L}^*)^{-1}\mathbf{R}^*, \quad \mathbf{B} = (\mathbf{L}^*)^{-1} \tag{69a,b}$$

$$\mathbf{E} = (\mathbf{L}^*)^{-1}\mathbf{L}_{\mathrm{s}}^*. \tag{69c}$$

For what concerns the output variables, posing

$$\mathbf{K} = \left(\frac{\partial \boldsymbol{y}}{\partial \psi}\, \frac{\partial \boldsymbol{y}}{\partial \boldsymbol{q}}\, \frac{\partial \boldsymbol{y}}{\partial \boldsymbol{s}}\right) \tag{70}$$

the matrices in Eq. (33) are given by

$$\mathbf{C} = \frac{\partial \boldsymbol{y}}{\partial \psi}\,\mathbf{G}_{11} + \frac{\partial \boldsymbol{y}}{\partial \boldsymbol{q}}\,\mathbf{G}_{21} \tag{71}$$

$$\mathbf{D} = \mathbf{0} \tag{72}$$

$$\mathbf{F}_{\mathrm{s}} = \frac{\partial \boldsymbol{y}}{\partial \psi}\,\mathbf{G}_{12} + \frac{\partial \boldsymbol{y}}{\partial \boldsymbol{q}}\,\mathbf{G}_{22} + \frac{\partial \boldsymbol{y}}{\partial \boldsymbol{s}}. \tag{73}$$

The derivation of the remaining matrices, introduced in Eqs (41), (43), (44) and (45), is straightforward.

## ACKNOWLEDGEMENTS

It is a pleasure to acknowledge Prof. G. Ambrosino and Prof. G. Rubinacci of the CREATE team, and Dr. A. Portone of ITER JCT, Naka, for stimulating discussions. The authors are also grateful to Dr. J.B. Lister and Dr. P. Vyas of CRPP, Lausanne, for reviewing the manuscript and for their invaluable cooperation in validating the model against experimental data.

The contribution of two unknown referees in making the presentation more readable is also acknowledged.

This work was partially supported by Euratom and MURST.

## REFERENCES

[1] LISTER, J.B., MARTIN, Y., MORET, J-M., Nucl. Fusion **36** (1996) 1547.
[2] SOLANO, E.R., NEILSON, G.H., LAO, L.L., Nucl. Fusion **30** (1990) 1107.
[3] HOFMANN, F., JARDIN, S.C., Nucl. Fusion **30** (1990) 2013.
[4] REBUT, P.H., et al., Fusion Eng. Des. **22** (1993) 7.
[5] DOYLE, J.C., STEIN, G., IEEE Trans. Autom. Control **AC-26** (1981) 4.
[6] MACIEJOWSKI, J.M., Multivariable Feedback Design, Addison-Wesley, Reading, MA (1989).
[7] JARDIN, S.C., POMPHREY, N., DE LUCIA, J., J. Comput. Phys. **66** (1986) 481.
[8] BLUM, J., LE FOLL, J., THOORIS, B., Comput. Phys. Commun. **24** (1981) 235.
[9] GRUBER, R., et al., Comput. Phys. Commun. **21** (1981) 323.
[10] WARD, D.J., JARDIN, S.C., CHENG, C.Z., J. Comput. Phys. **104** (1993) 221.
[11] ALBANESE, R., COCCORESE, E., RUBINACCI, G., Nucl. Fusion **29** (1989) 1013.
[12] HUMPHREY, D.A., HUTCHINSON, I.H., Fusion Technol. **23** (1993) 167.
[13] ALBANESE, R., et al., Fusion Technol. **30** (1996) 167.
[14] GARRIBBA, M., et al., in Fusion Technology (Proc. 18th Symp. Karlsruhe, 1994), Elsevier, Amsterdam and New York (1995) 747.
[15] LUXON, J.L., BROWN, B.B., Nucl. Fusion **22** (1982) 813.
[16] ALBANESE, R., RUBINACCI, G., in Computation and Applied Mathematics (Proc. 13th IMACS World Congress Dublin, 1991), Trinity College, Dublin (1991) 1618.
[17] FREIDBERG, J.P., Ideal Magnetohydrodynamics, Plenum Press, New York and London (1985) 264.
[18] STRAIT, E.J., LAO, L.L., LUXON, J.L., REIS, E.E., Nucl. Fusion **31** (1991) 527.
[19] ALBANESE, R., in Fusion Technology (Proc. 15th Symp. Utrecht, 1988), Vol. 1, Elsevier, Amsterdam and New York (1989) 281.
[20] ALBANESE, R., Time Evolution of a Magnetically Confined Plasma, PhD Thesis, Univ. of Naples (1986) (in Italian).
[21] ALBANESE, R., BLUM, J., DE BARBIERI, O., "Numerical Studies of the Next European Torus via the PROTEUS code", paper presented at the 12th Conf. on Numerical Simulation of Plasmas, San Francisco, 1987.
[22] ALBANESE, R., et al., "Contribution of CREATE to the EUHT activity on ITER Tasks D255 and D324-1", paper presented at the 3rd Plasma Control Task Force Meeting, ITER JWS, Naka, 1996.

[23] VILLONE, F., VYAS, P., LISTER, J.B., ALBANESE, R., Nucl. Fusion **37** (1997) 1395.
[24] WALKER, M.L., et al., "Simulation and assessment of linear controllers: GA/LLNL and CREATE models/controllers", paper presented at the ITER Control Design Task D324 Review Mtg, ITER JWS, Garching, 1997.
[25] LODESTRO, L.L, PEARLSTEIN, L.D., Phys. Plasmas **1** (1994) 90.
[26] BARABASCHI, P., ITER JWS, San Diego, CA, personal communication, 1993.
[27] ALBANESE, R., et al., "Modelling and engineering aspects of the plasma shape control in ITER", paper presented at the 19th Symp. on Fusion Technology, Lisbon, 1996.
[28] MARCHIORI, G., "Simulation of the open loop plasma response with the non-linear MHD code MAXFEA", paper presented at the ITER Control Design Task D324 Review Mtg, ITER JWS, Garching, 1997.

(Manuscript received 6 June 1997
Final manuscript accepted 5 February 1998)

E-mail address of R. Albanese:
albanese@disna.dis.unina.it

Subject classification: E0, Tt; C0, Tt